Nanoparticle Conjugation Stabilizes and Multimerizes β-Hairpin Peptides to Effectively Target PD-1/PD-L1 β-Sheet-Rich Interfaces

Woo-jin Jeong,† Jiyoon Bu,† Yanxiao Han,‡ Adam J. Drelich,† Ashita Nair,† Petr Král,‡,⊥,§ and Seungpyo Hong†,∥,¶,*

†Pharmaceutical Sciences Division and ∥Department of Biomedical Engineering, The University of Wisconsin-Madison, 777 Highland Ave., Madison, WI 53705, USA

¶Yonsei Frontier Lab, Department of Pharmacy, Yonsei University, Seoul 03722, Republic of Korea.

‡Departments of Chemistry, ⊥Physics, and §Biopharmaceutical Sciences, University of Illinois at Chicago, Chicago, Illinois 60607, USA.

KEYWORDS. Peptide-dendrimer conjugate, β-hairpin stabilization, Multivalent binding, Immune checkpoint blockade, Cancer immunotherapy

ABSTRACT: β-hairpin peptides present great potential as antagonists against β-sheet-rich protein surfaces, of which wide and flat geometries are typically 'undruggable' with small molecules. Herein, we introduce a peptide-dendrimer conjugate (PDC) approach that stabilizes β-hairpin structure of the peptide via intermolecular forces and excluded volume effect as well as exploits multivalent binding effect. Due to the synergistic advantages, the PDCs based on a β-hairpin peptide isolated from an engineered programmed death-1 (PD-1) protein showed significantly higher affinity (avidity) to their binding counterpart, programmed death-ligand 1 (PD-L1), compared to free peptides (by up to 5 orders of magnitude). The enhanced binding kinetics with high selectivity was translated into an improved immune checkpoint inhibitory effect in vitro, at a level comparable to (if not better than) a full-size monoclonal antibody. The results demonstrate the potential of the PDC system as a novel class of inhibitors targeting β-strand-rich protein surfaces, such as PD-1 and PD-L1, displaying its potential as a new cancer immunotherapy platform.

PD-1, an immunoinhibitory receptor expressed on activated T cells, and its ligand, PD-L1 that is often expressed by tumor cells, have gained increasing interest as targets for cancer immunotherapy.[1,2] The blockade of their interaction that halts or limits T cell response results in the reactivation of anticancer immunity and, in turn, tumor regression.[3] Because it is challenging for small molecules to antagonize the wide and flat interfaces of protein-protein interactions (PPIs),[4] the majority of anti PD-1/PD-L1 agents currently approved or under development are based on full-size monoclonal antibodies. Despite their demonstrated efficacy, the widespread use of the antibody drugs has been hindered due to their high cost and complexity in manufacturing and low thermodynamic stability.[5,6] In addition, having many functional groups (e.g. amine, carboxyl, and sulfhydryl groups), antibodies are not compatible with site-specific chemical modifications or conjugations with other materials (e.g. small molecules, polymers, nanoparticles, and biomolecules), which further limits their use in advanced biomedical applications.

Molecularly poised between small molecules and proteins, peptides hold great potential as PPI inhibitors without the aforementioned disadvantages of the both.[7] The use of peptide segments on protein surfaces is one of the promising approaches to achieve high target affinity and selectivity.[8] However, peptides isolated from protein contexts cannot typically maintain their innate folding structures, which frequently leads to altering their physicochemical properties and thereby substantially reducing their binding capabilities.[9] For this reason, many attempts, such as the stapled peptide approach, molecular self-assembly, and bio-inorganic hybridization, have been made to stabilize the molecular conformations in short peptides.[10-12] Although some of the strategies targeting α-helical interfaces have produced successful results, the development of peptide antagonists that effectively block β-sheet-rich protein surfaces, where multiple β-strands are displayed on a wide and flat geometry, remains elusive.[13] Because such surfaces are ubiquitous in PPIs and play a critical role in the progress of protein aggregation-related diseases, control of PPIs mediated by β-sheet-rich surfaces has been an important and challenging issue in pharmaceutical research.[14]

In the present study, to develop a novel PD-1/PD-L1 inhibitor targeting their β-sheet-rich interface, we isolated β-hairpin peptides from the PD-1 surface and engineered them through a combination of three synergistic approaches (Figure 1a). First, we used the amino acid composition of an unnatural PD-1 ectodomain optimized to exhibit high PD-L1 affinity by Maute et al.[15,16] Second, the peptides were conjugated to dendrimer surfaces in a multivalent fashion, thereby enabling cooperative, strong interactions with multiple PD-L1 proteins on tumor cells. Third, the conjugation on a dendrimer surface assisted peptide folding into their native structure, β-hairpin, due to the excluded volume effect and the peptide-dendrimer interactions.[17] Considering the potential synergetic effect of these engineering approaches, we thus hypothesized that this PDC strategy would enable the peptides to outperform natural PD-1 in competitive interaction with PD-L1 for the recovery of antitumor immunity.

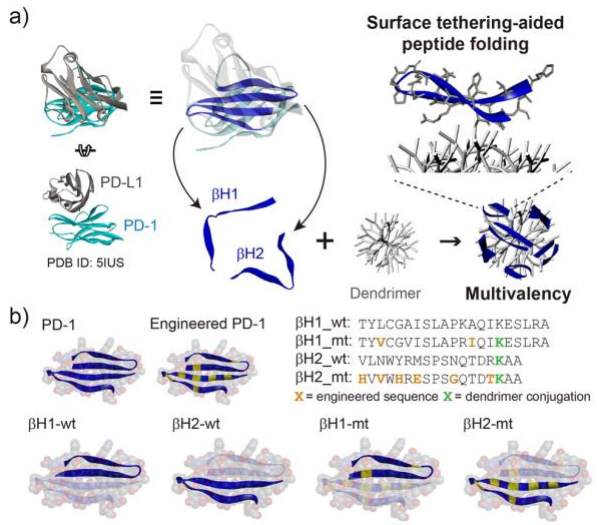

Figure 1. (a) Schematic illustration of the development process of a multivalent dendrimer-peptide conjugate as a PD-1/PD-L1 antagonist. (b) 3D structures of PD-1, engineered PD-1, and 4 peptides with the binding surfaces highlighted (blue ribbon), along with the full sequences of the 4 peptides.

To develop PD-L1-targeted PDCs, β-hairpin peptides were synthesized based on the engineered PD-1 ectodomain sequence that was reported elsewhere (βH1_mt and βH2_mt, Figure 1b),[15,16] and attached to the surface of generation seven (G7) poly(amidoamine) (PAMAM) dendrimers. Note that the peptide sequences were partially modified for the dendrimer conjugation, as described in Figure S1. Before the conjugation, 90% of dendrimer amine groups were acetylated to control the number of attached peptides, given that surface area of G7 PAMAM dendrimers is approximately ten times larger than that of PD-1/PD-L1 interface (Figure 2a). The resulting PDCs, noted as G7-βH1_mt and G7-βH2_mt, were then analyzed using surface plasmon resonance (SPR) to measure their binding kinetics. As shown in Figure 2b, G7-βH2_mt exhibited higher affinity to immobilized PD-L1 proteins than G7-βH1_mt, whereas fully acetylated dendrimers showed no binding response. Additionally, the PD-L1 affinity of G7-βH2_mt was also higher than that of the wildtype βH2-dendrimer conjugate control (G7-βH2_wt), indicating that the engineered PD-1 sequence (βH2_mt) leads to the higher affinity. Hence, we selected βH2_mt peptides as the PD-L1-targeted ligand and conjugated them to dendrimer surfaces with varying degrees of acetylation to determine effective peptide valency. One can expect that the binding strength as a results of multivalent binding interaction would be proportional to the number of ligand molecules.[18-22] However, lower PD-L1 affinity was observed for the PDCs with greater numbers of βH2_mt peptides (i.e. the PDCs prepared from 80% and 60% acetylated dendrimers) (Figure 2c, S4, and S5). These unexpected results are probably attributed to the fact that the optimized spatial distance among ligands plays a key role in achieving stronger binding, rather than a mere increase in the number of ligands, which was also observed elsewhere.[23,24] These results collectively indicate that G7-βH2_mt prepared from 90% acetylated dendrimers would likely antagonize the PD-1/PD-L1 interaction more effectively than its counterparts, G7-βH1_mt and G7-βH2_wt.

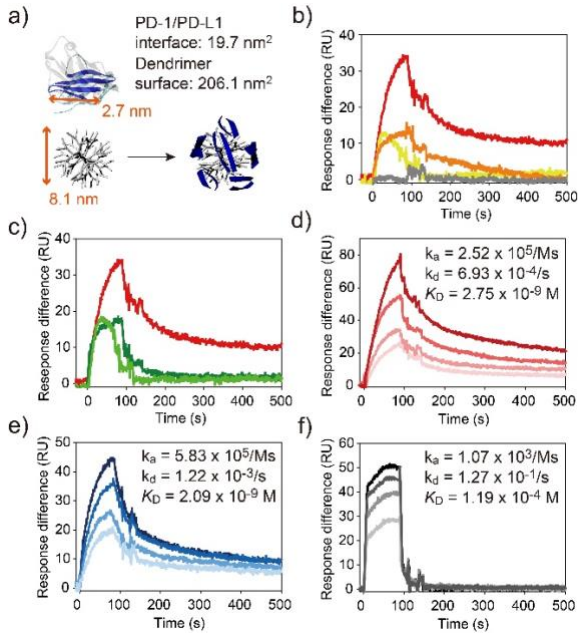

Figure 2. (a) Size comparison among the βH2_mt peptide, G7 PAMAM dendrimer, and PD-1/PD-L1 interface, indicating that the dendrimer surface accommodates multiple peptides being separated by enough spatial distance for binding. (b) SPR sensorgrams for binding of G7-βH2_mt (red), G7-βH2_wt (orange), G7-βH1_mt (yellow), and fully acetylated dendrimers (gray) to immobilized PD-L1 proteins. (c) SPR sensorgrams for binding of G7-βH2_mt conjugates using 90% (red), 80% (dark green), and 60% (light green) acetylated dendrimers to PD-L1. Concentration dependent binding kinetics of (d) G7-βH2_mt conjugates (45/90/180/270 nM) (e) aPD-L1 antibodies (25/50/100/200 nM), and (f) free βH2_mt peptides (17/25/33/42 μM) to PD-L1.

Next, we compared the PD-L1 binding kinetics of G7-βH2_mt with that of anti-PD-L1 (aPD-L1) antibodies and free βH2_mt peptides. The SPR analysis revealed that G7-βH2_mt showed five orders of magnitude higher PD-L1 affinity than βH2_mt (K_D of 2.75×10^{-9} vs. 1.19×10^{-4}), which is comparable to that of whole aPD-L1 antibody (K_D of 2.09×10^{-9}), as shown in Figure 2d, 2e, and 2f. It is noteworthy that the dissociation rate constant (k_d) of G7-βH2_mt was decreased by ~180 times, compared to the free peptide, although there were only 30 peptides per dendrimer (Figure S5). This non-linear enhancement in binding is characteristic of multivalent binding effect, i.e. a multivalent object has a higher rebinding chance to target molecules than its monovalent counterpart (statistical rebinding mechanism).[25,26] Interestingly, association rate constant (k_a), which is known to play a minor role in the multivalent binding effect,[18] also increased non-linearly (2.52×10^5 vs. 1.07×10^3). This result implies that other factors, in addition to the multivalent binding, contribute to the significantly enhanced PD-L1 binding of G7-βH2_mt.

To elucidate the mechanism behind the improved binding kinetics of G7-βH2_mt, we investigated the folding structure change of the peptides, which significantly affects their target affinity and selectivity,[27,28] upon conjugation to dendrimers. Figure 3a shows the circular dichroism (CD) profile of G7-βH2_mt (red line) where a degree of peptide folding was observed (the negative signal at ~220 nm), which is distinct from the typical CD spectra of other possible peptide folding

structures, such as α-helix (broad negative band centered 222 nm), 3_{10} helix, triple helix, and turn.[29-31] In contrast, free βH2_mt displayed an almost unfolded random-coil structure (black line), as shown in the strong negative CD band at ~200 nm. Note that the CD profiles for dendrimers (both red and gray lines) omitted the signal below 218 nm due to the abundant amide bonds in the dendrimer backbones absorbing far ultraviolet (UV) light. A concentration of 1 μM of dendrimers was used to minimize the absorption of low wavelength light by the macromolecules and yet to obtain strong enough signals for data interpretation in a range of 190-230 nm where the secondary structure of peptides is typically characterized.

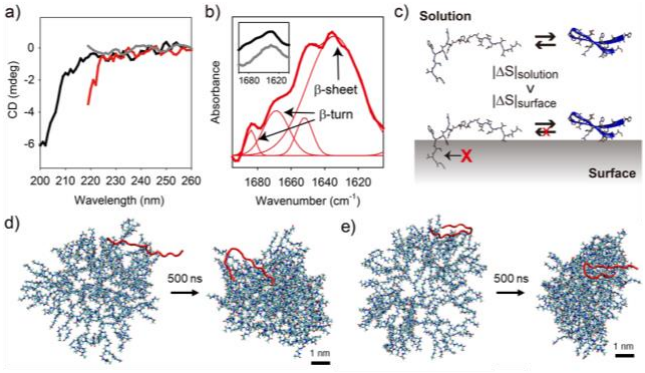

Figure 3. (a) CD spectra of G7-βH2_mt conjugates (red), βH2_mt peptides (black) and fully acetylated dendrimers (gray). (b) FTIR spectra of G7-βH2_mt conjugates (thick red) and its Fourier self-deconvolution analysis (thin red). Inset: FTIR spectra of βH2_mt peptides (black) and fully acetylated dendrimers (gray). (c) Schematic illustration of the excluded volume effect that decreases entropy cost for peptide folding. MD simulation results of the folding behaviors of βH2_mt upon conjugation with a G5 PAMAM dendrimer: (d) initially extended βH2_mt vs. (e) initially folded βH2_mt (βH2_mt in red ribbon, atoms in G5: oxygen in red, carbon in cyan, nitrogen in blue and hydrogen in white)

We then employed the attenuated total reflection-Fourier transform Infrared (ATR-FTIR) to study the folding behaviors of the peptides. As shown in Figure 3b, the FTIR spectra confirmed the presence of random coil and β-sheet (a broad band around 1640 cm^{-1}), along with a trace of β-turn structures (weak absorption around 1670 and 1690 cm^{-1}), in βH2_mt peptides.[32,33] In contrast, the FTIR spectrum of G7-βH2_mt displayed the signature of a β-hairpin structure with resolvable absorption at 1634 cm^{-1} for inter-strand vibrational couplings and 1668 and 1683 cm^{-1} for β-turn conformation. Therefore, both of the structural analyses collectively show that the hairpin structure of βH2_mt is stabilized by the dendrimer conjugation. These results are in agreement with several theoretical studies suggesting that surface tethering allows the stabilization of biomolecular structures via the excluded volume effect (Figure 3c), i.e., in the presence of a substrate, conformational freedom of a peptide to be unfolded is limited, resulting in reduced entropy cost for folding.[17,34]

To support the experimental results, we performed molecular dynamics (MD) simulations using a single βH2_mt peptide-generation five (G5) PAMAM dendrimer conjugate. Note that G5 PAMAM dendrimer, instead of larger G7, was used for efficient computing time. The peptide behaviors on the surface of a dendrimer were compared for 500 ns from initially (1) extended and (2) folded βH2_mt (Figure 3d and 3e). βH2_mt in physiological solution is also illustrated in Figure S6a. In contrast to free βH2_mt exhibiting both folded and extended conformations in the solution, the initially extended peptide bent to a folded structure and initially folded βH2_mt stably maintained the folded conformation on the dendrimer surface. Interestingly, the peptide generated various intermolecular forces with the dendrimer surface, including hydrogen bonds, electrostatic interactions, and van der Waals interactions, while maintaining the hairpin structure (Figure S6b and S6c). In general, formation of such molecular interactions with a surface is known to reduce the structural stability of proteins.[35] However, βH2_mt is an isolated peptide segment that is originally exposed to multiple molecular interactions within the entire PD-1 protein structure (Figure S7). These molecular interactions seem to contribute to the further stabilization of the peptide molecule in a folded conformation on the dendrimer surface, in addition to the reduced entropy cost described above.

The best way to stabilize β-hairpin is the covalent cross-linking of the two strands in a peptide.[36] However, chemical modifications typically complicate the peptide preparation process and, in turn, induce a significant decrease in synthetic yield.[37] The introduction of inter-strand noncovalent binding is another commonly used strategy; however, it requires substantial amino acid substitutions, which potentially affects physicochemical properties of the peptide.[36] On the contrary, our PDC strategy allows to stabilize the hairpin structure of peptides with minimal modifications to the peptide structure. Combined with the multivalent binding advantages endowed from the dendritic nanoparticles, this unique PDC platform presents a novel way to effectively antagonize and target β-sheet-rich protein surfaces.

Next, we investigated the possibility of using G7-βH2_mt as a PD-1/PD-L1 inhibitor. To perform a fluorescence polarization (FP) competition assay, fluorescein-conjugated βH2_mt (fβH2_mt) peptides were synthesized and used to construct target complexes with PD-L1 proteins (Figure 4a). In the competition experiment (fβH2_mt, 10 nM; PD-L1, 2 μM), the complex integrity was not affected by the addition of βH2_mt peptides and fully acetylated dendrimers, whereas G7-βH2_mt resulted in a dose-dependent displacement of fβH2_mt from PD-L1 (Figure 4b). Interestingly, the PDC showed a more effective competitiveness than aPD-L1 antibodies despite the slightly lower PD-L1 affinity, which can be attributed to the multivalent ligand display that allows the accommodation of multiple target proteins on a PDC surface (Figure 4c). Furthermore, compared to a previously-reported nanostructure decorated with stabilized and densely multimerized α-helices,[38] our PDC showed significantly greater improvement in the inhibitory effect, likely due to the optimized spatial distance between peptides on the dendrimer surface.

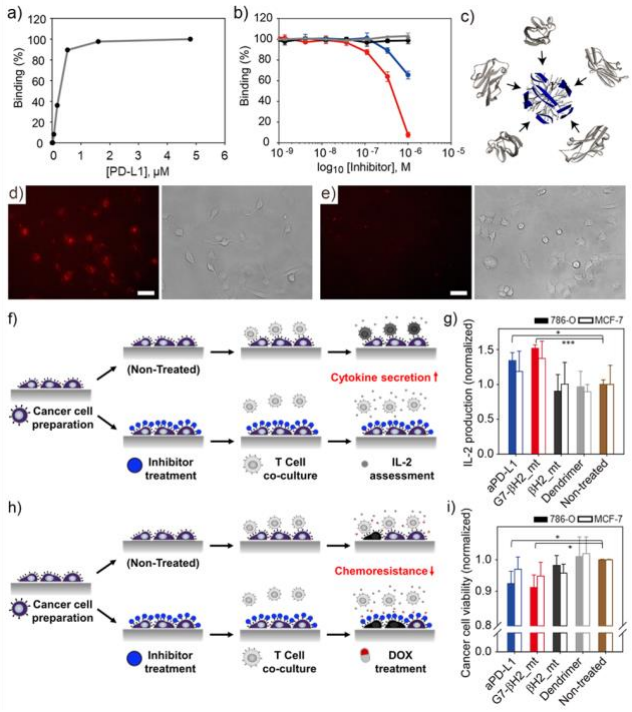

Figure 4. Binding studies using FP spectroscopy: (a) Binding of fβH2_mt to PD-L1; and (b) Competition assays on G7-βH2_mt (red), aPD-L1 (blue), βH2_mt (black), and fully acetylated dendrimer (gray) against fβH2_mt/PD-L1 complexes. (c) Illustration of a G7-βH2_mt conjugate binding to multiple PD-L1 proteins. Fluorescence microscopy images of (d) 786-O and (e) MCF-7 cells treated with G7-βH2_mt for 1h (red fluorescence from Rhodamine, left; bright field image, right), scale bar: 50 μm. Schematic illustration of immune checkpoint blockade resulting in (f) increased interlukin-2 (IL-2) secretion by Jurkat T cells and (h) reduction of cancer cell chemoresistance. (g) IL-2 secretion from Jurkat T cells co-cultured with 786-O and MCF-7 cells after treated with various groups. (i) Cancer cell viability after doxorubicin (DOX) treatment, demonstrating the chemoresistance of the cancer cells upon incubation with various groups (*p ≤ 0.05, ***p ≤ 0.001).

To further scrutinize their efficiency, the PDCs were then tested *in vitro*. As shown in Figure 4d, 4e, and S8, strong cell interactions of G7-βH2_mt with 786-O cells (a PD-L1 overexpressing cell line) were observed using a fluorescence microscope, whereas the PDCs interacted significantly less with MCF-7 cells (with a low level of PD-L1 expression), demonstrating high PD-L1 selectivity of G7-βH2_mt. This minimal non-specific interaction also indicates that all the terminal amine groups of starting G7 dendrimers were successfully acetylated or consumed for the peptide conjugation.[39,40] The *in vitro* PD-1/PD-L1 inhibitory effect was then assessed by measuring the amount of cytokines (interleukin-2, IL-2) secreted by Jurkat T cells after being co-cultured with the cancer cells, as described elsewhere (Figure 4f).[41] The blockade of PD-1/PD-L1 binding is well known to activate T cells and promote their cytokine production.[42] Figure 4g shows that G7-βH2_mt effectively inhibited the 786-O/Jurkat T cell interaction, resulting in an increased IL-2 secretion from the T cells by 1.52-fold ($p < 0.001$) compared with the non-treated cancer cells, which was even more pronounced than aPD-L1 antibodies that showed a 1.34-fold enhancement ($p = 0.011$) only. This could be attributed to the multivalent binding effect of G7-βH2_mt. Note that neither free peptides nor fully acetylated dendrimers induced noticeable IL-2 production.

To corroborate the PD-1/PD-L1 inhibition, we also tested if the PDC treatment can affect chemoresistance of cancer cells, which is proven to be reduced by immune checkpoint blockade in many clinical and pre-clinical studies.[43-45] A co-culture model using tumor (786-O or MCF-7) and Jurkat T cells was employed to investigate the synergistic cytotoxic effect of doxorubicin (DOX) and G7-βH2_mt (Figure 4h).[46] Cancer cells treated with different PD-L1 antagonists were co-cultured with the T cells, followed by DOX treatment (5 μM) to induce cell death. As shown in Figure 4i, blocking PD-L1 molecules with G7-βH2_mt significantly reduced the chemoresistance of 786-O cells, exhibiting a decreased cell viability by 8.4 ± 3.8%, compared to the cells treated with doxorubicin only ($p = 0.022$). This synergistic effect of the DOX and PDC treatments is intriguing, considering that only ~12.4% of reduced cell viability was observed despite the 4X dose of free DOX (20 μM) used, as shown in the concentration-dependent cell viability data (Figure S9). In addition, G7-βH2_mt was slightly more effective than the aPD-L1 antibodies that induced a 7.2 ± 3.7% cell viability reduction ($p = 0.030$). As the free peptides only have a minor effect on the chemoresistance (1.8 ± 2.0% reduction; $p = 0.334$) and fully acetylated G7 dendrimers have no cytotoxic effect on the cancer cells, this result provides another layer of evidence that multivalent G7-βH2_mt effectively blocks the PD-1/PD-L1 immune checkpoint. MCF-7 cells, expressing a low level of PD-L1, also exhibited a similar tendency, although the differences were not as significant as the high PD-L1 expressing 786-O cells. The observed cytotoxicity in this experiment was attributed to the apoptotic mechanism caused by DOX, as shown in Figure S9c.

In conclusion, we have demonstrated that the PDC approach enables β-hairpin peptides isolated from protein surfaces to be multimerized and conformationally stabilized on nanoscale dendrimers, thereby exhibiting significantly enhanced target affinity. The enhanced binding kinetics was translated into a significant enhancement of *in vitro* efficiency where the PDCs exhibited dramatically stronger PD-1/PD-L1 inhibitory effect than the free peptides and a comparable level of efficiency to aPD-L1 antibodies. The PD-L1 inhibition using antibodies has already been clinically proven effective in treating several cancer types, such as non-small lung cancer, bladder cancer, and Merkel cell skin cancer.[47] However, the currently approved antagonists based on monoclonal antibodies have limitations due to their high cost and a lack of modularity.[1,48] Our strategy has potential to address these problems, because the dendrimer-peptide system offers a platform technology that can accommodate not only immunotherapy but other antitumor agents as well.[49] Furthermore, a variety of β-hairpin peptides on many protein surfaces could be compatible with this PDC approach, increasing its potential to be used in diverse biomedical applications. This study provides a newly engineered peptide-nanoparticle platform for effective regulation of protein interactions to tackle various diseases, including immune checkpoint blockade for cancer therapy.

ASSOCIATED CONTENT

Supporting Information.
Experimental details and characterization data of the peptides and PDCs, including Figures S1-S7. This material is available free of charge via the Internet at http://pubs.acs.org.

AUTHOR INFORMATION

Corresponding Author

* seungpyo.hong@wisc.edu

Notes

The authors declare no competing financial interest.

ACKNOWLEDGMENT

This study was partially supported by National Science Foundation (NSF) under grant # DMR-1808251. The authors also acknowledge the partial support from NIAMS/NIH under grant # 1R01AR069541 and NIBIB/NIH under grant # 1R21EB022374.

REFERENCES

(1) Ribas, A.; Wolchok, J. D. *Science* **2018**, *359*, 1350.
(2) Tang, J.; Yu, J. X.; Hubbard-Lucey, V. M.; Neftelinov, S. T.; Hodge, J. P.; Lin, Y. *Nat. Rev. Drug discovery* **2018**, *17*, 854.
(3) Tang, H. D.; Liang, Y.; Anders, R. A.; Taube, J. M.; Qiu, X. Y.; Mulgaonkar, A.; Liu, X.; Harrington, S. M.; Guo, J. Y.; Xin, Y. C.; Xiong, Y. H.; Nham, K.; Silvers, W.; Hao, G. Y.; Sun, X. K.; Chen, M. Y.; Hannan, R.; Qiao, J.; Dong, H. D.; Peng, H.; Fu, Y. X. *J. Clin. Invest.* **2018**, *128*, 580.
(4) Crews, C. M. *Chem. Biol.* **2010**, *17*, 551.
(5) Leader, B.; Baca, Q. J.; Golan, D. E. *Nat. Rev. Drug Discovery* **2008**, *7*, 21.
(6) Klutz, S.; Holtmann, L.; Lobedann, M.; Schembecker, G. *Chem. Eng. Sci*. **2016**, *141*, 63.
(7) Lau, J. L.; Dunn, M. K. *Bioorg. Med. Chem.* **2018**, *26*, 2700.
(8) Jeong, W. J.; Choi, S. H.; Jin, K. S.; Lim, Y. B. *Acs Macro Lett.* **2016**, *5*, 1406.
(9) Klein, M. *Expert Opin. Drug Dis.* **2017**, *12*, 1117.
(10) Jeong, W. J.; Choi, S. J.; Choi, J. S.; Lim, Y. B. *ACS nano* **2013**, *7*, 6850.
(11) Carvajal, L. A.; Ben Neriah, D.; Senecal, A.; Benard, L.; Thiruthuvanathan, V.; Yatsenko, T.; Naraya-nagari, S. R.; Wheat, J. C.; Todorova, T. I.; Mitchell, K.; Kenworthy, C.; Guerlavais, V.; Annis, D. A.; Bartholdy, B.; Will, B.; Anampa, J. D.; Mantzaris, I.; Aivado, M.; Singer, R. H.; Coleman, R. A.; Verma, A.; Steidl, U. *Sci Transl. Med.* **2018**, *10*, eaao3003.
(12) Jeong, W. J.; Han, S.; Park, H.; Jin, K. S.; Lim, Y. B. *Biomacromolecules* **2014**, *15*, 2138.
(13) Watkins, A. M.; Arora, P. S. *ACS Chem. Biol.* **2014**, *9*, 1747.
(14) Cheng, P. N.; Pham, J. D.; Nowick, J. S. *J. Am. Chem. Soc.* **2013**, *135*, 5477.
(15) Maute, R. L.; Gordon, S. R.; Mayer, A. T.; McCracken, M. N.; Natarajan, A.; Ring, N. G.; Kimura, R.; Tsai, J. M.; Manglik, A.; Kruse, A. C.; Gambhir, S. S.; Weissman, I. L.; Ring, A. M. *Proc. Nat. Acad. Sci. USA* **2015**, *112*, E6506.
(16) Pascolutti, R.; Sun, X. Q.; Kao, J.; Maute, R. L.; Ring, A. M.; Bowman, G. R.; Kruse, A. C. *Structure* **2016**, *24*, 1719.
(17) Knotts, T. A.; Rathore, N.; de Pablоz, J. J. *Biophys. J.* **2008**, *94*, 4473.
(18) Hong, S.; Leroueil, P. R.; Majoros, I. J.; Orr, B. G.; Baker, J. R., Jr.; Banaszak Holl, M. M. *Chem. Biol.* **2007**, *14*, 107.
(19) Sen, S.; Han, Y.; Rehak, P.; Vukovic, L.; Kral, P. *Chem. Soc. Rev.* **2018**, *47*, 3849.
(20) Cagno, V.; Andreozzi, P.; D'Alicarnasso, M.; Silva, P. J.; Mueller, M.; Galloux, M.; Le Goffic, R.; Jones, S. T.; Vallino, M.; Hodek, J.; Weber, J.; Sen, S.; Janecek, E. R.; Bekdemir, A.; Sanavio, B.; Martinelli, C.; Donalisio, M.; Welti, M. A. R.; Eleouet, J. F.; Han, Y. X.; Kaiser, L.; Vukovic, L.; Tapparel, C.; Kral, P.; Krol, S.; Lembo, D.; Stellacci, F. *Nat. Mater.* **2018**, *17*, 195.
(21) Myung, J. H.; Eblan, M. J.; Caster, J. M.; Park, S. J.; Poellmann, M. J.; Wang, K.; Tam, K. A.; Miller, S. M.; Shen, C.; Chen, R. C.; Zhang, T.; Tepper, J. E.; Chera, B. S.; Wang, A. Z.; Hong, S. *Clin. Cancer Res.* **2018**, *24*, 2539.
(22) Myung, J. H.; Gajjar, K. A.; Saric, J.; Eddington, D. T.; Hong, S. *Angew. Chem. Int. Edit.* **2011**, *50*, 11769.
(23) Kwon, S. J.; Na, D. H.; Kwak, J. H.; Douaisi, M.; Zhang, F.; Park, E. J.; Park, J. H.; Youn, H.; Song, C. S.; Kane, R. S.; Dordick, J. S.; Lee, K. B.; Linhardt, R. J. *Nat. Nanotechnol.* **2017**, *12*, 48.
(24) Lauster, D.; Glanz, M.; Bardua, M.; Ludwig, K.; Hellmund, M.; Hoffmann, U.; Hamann, A.; Bottcher, C.; Haag, R.; Hackenberger, C. P. R.; Herrmann, A. *Angew. Chem. Int. Edit.* **2017**, *56*, 5931.
(25) Jeong, W. J.; Bu, J.; Kubiatowicz, L. J.; Chen, S. S.; Kim, Y.; Hong, S. *Nano Converg.* **2018**, *5*, 38.
(26) Qian, E. A.; Wixtrom, A. I.; Axtell, J. C.; Saebi, A.; Jung, D. H.; Rehak, P.; Han, Y. X.; Moully, E. H.; Mosallaei, D.; Chow, S.; Messina, M. S.; Wang, J. Y.; Royappa, A. T.; Rheingold, A. L.; Maynard, H. D.; Kral, P.; Spokoyny, A. M. *Nat. Chem.* **2017**, *9*, 333.
(27) Verhoork, S. J. M.; Jennings, C. E.; Rozatian, N.; Reeks, J.; Meng, J.; Corlett, E. K.; Bunglawala, F.; Noble, M. E. M.; Leach, A. G.; Coxon, C. R. *Chemistry* **2019**, *25*, 177.
(28) Butterfield, S. M.; Waters, M. L. *J. Am. Chem. Soc.* **2003**, *125*, 9580.
(29) Micsonai, A.; Wien, F.; Kernya, L.; Lee, Y. H.; Goto, Y.; Refregiers, M.; Kardos, J. *Proc. Nat. Acad. Sci. USA* **2015**, *112*, E3095.
(30) Singh, Y.; Sharpe, P. C.; Hoang, H. N.; Lucke, A. J.; McDowall, A. W.; Bottomley, S. P.; Fairlie, D. P. *Chem. Eur. J.* **2011**, *17*, 151.
(31) Greenfield, N. J. *Nat. Protoc.* **2006**, *1*, 2527.
(32) Du, D. G.; Zhu, Y. J.; Huang, C. Y.; Gai, F. *Proc. Nat. Acad. Sci. USA* **2004**, *101*, 15915.
(33) Jun, S.; Hong, Y.; Imamura, H.; Ha, B. Y.; Bechhoefer, J.; Chen, P. *Biophys. J.* **2004**, *87*, 1249.
(34) Watkins, H. M.; Vallee-Belisle, A.; Ricci, F.; Makarov, D. E.; Plaxco, K. W. *J. Am. Chem. Soc.* **2012**, *134*, 2120.
(35) Kurnik, M.; Ortega, G.; Dauphin-Ducharme, P.; Li, H.; Caceres, A.; Plaxco, K. W. *Proc. Nat. Acad. Sci. USA* **2018**, *115*, 8352.
(36) Morales, P.; Jimenez, M. A. *Arch. Biochem. Biophys.* **2019**, *661*, 149.
(37) Choi, S. H.; Jeong, W. J.; Choi, S. J.; Lim, Y. B. *Bioorg. Med. Chem. Lett.* **2015**, *25*, 5335.
(38) Jeong, W. J.; Lee, M. S.; Lim, Y. B. *Biomacromolecules* **2013**, *14*, 2684.
(39) Hsu, H. J.; Sen, S.; Pearson, R. M.; Uddin, S.; Kral, P.; Hong, S. *Macromolecules* **2014**, *47*, 6911.
(40) Pearson, R. M.; Patra, N.; Hsu, H. J.; Uddin, S.; Kral, P.; Hong, S. *ACS Macro Lett.* **2013**, *2*, 77.
(41) Yang, W.; Chen, P. W.; Li, H.; Alizadeh, H.; Niederkorn, J. Y. *Invest. Ophthalmol. Vi.s Sci.* **2008**, *49*, 2518.
(42) Shi, L.; Chen, S.; Yang, L.; Li, Y. *J. Hematol. Oncol.* **2013**, *6*, 74.
(43) Yan, Y.; Kumar, A. B.; Finnes, H.; Markovic, S. N.; Park, S.; Dronca, R. S.; Dong, H. *Front. Immunol.* **2018**, *9*, 1739.
(44) Grasselly, C.; Denis, M.; Bourguignon, A.; Talhi, N.; Mathe, D.; Tourette, A.; Serre, L.; Jordheim, L. P.; Matera, E. L.; Dumontet, C. *Front. Immunol.* **2018**, *9*, 2100.
(45) Wu, X. S.; Li, Y. L.; Liu, X.; Chen, C. H.; Harrington, S. M.; Cao, S. Y.; Xie, T. C.; Orzechowski, A.; Pham, T.; Mansfield, A. S.; Yan, Y. Y.; Kwon, E. D.; Wang, L. W.; Ling, K.; Dong, H. D. *Heliyon* **2018**, *4*. E01039.
(46) Black, M.; Barsoum, I. B.; Truesdell, P.; Cotechini, T.; Macdonald-Goodfellow, S. K.; Petroff, M.; Siemens, D. R.; Koti, M.; Craig, A. W.; Graham, C. H. *Oncotarget* **2016**, *7*, 10557.
(47) Bellmunt, J.; Powles, T.; Vogelzang, N. J. *Cancer Treat. Rev.* **2017**, *54*, 58.
(48) Verma, V.; Sprave, T.; Haque, W.; Simone, C. B., 2nd; Chang, J. Y.; Welsh, J. W.; Thomas, C. R., Jr. *J. Immunother. Cancer* **2018**, *6*, 128.
(49) Bugno, J.; Hsu, H. J.; Hong, S. *Biomater. Sci.* **2015**, *3*, 1025.

Table of Contents artwork